MS JNP 17102P-R revised (oct 17th, 2017)

Vapor and Liquid Optical Monitoring with Sculptured Bragg Microcavities

Manuel Oliva-Ramirez*, Jorge Gil-Rostra, Maria C. López-Santos, Agustín R. González-Elipe, Francisco Yubero*

Instituto de Ciencia de Materiales de Sevilla (CSIC, University of Seville) , CICCartuja, Avda. Américo Vespucio 49, E-41092, Spain

Abstract. Sculptured porous Bragg Microcavities (BMs) formed by the successive stacking of columnar SiO_2 and TiO_2 thin films with a zig-zag columnar microstructure are prepared by glancing angle deposition. These BMs act as wavelength dependent optical retarders. This optical behavior is attributed to a self-structuration of the stacked layers involving the lateral association of nanocolumns in the direction perpendicular to the main flux of particles during the multilayer film growth, as observed by Focused Ion Beam Scanning Electron Microscopy. The retardance of these optically active BMs can be modulated by dynamic infiltration of their open porosity with vapors, liquids or solutions with different refractive indices. The tunable birefringence of these nanostructured photonic systems have been successfully simulated with a simple model that assumes that each layer within the BMs stack has uniaxial birefringence. The sculptured BM have been incorporated as microfluidic chips for optical transduction for label free vapor and liquid

sensing. Several examples of the detection performance of these chips, working either in reflection or transmission configuration, for the optical monitoring of vapor and liquids of different refractive index and aqueous solutions of glucose flowing through the microfluidic chips are described.

Keywords: Sculptured thin films, porous films, Bragg Microcavities, optofluidics, vapor sensing, liquid sensing.

***Francisco Yubero**, E-mail: yubero@icmse.csic.es

*Manuel Oliva-Ramírez, Email: manuel.oliva@icmse.csic.es

1 Introduction

Thin film growth by physical vapor deposition methods such as electron beam, ion-beam evaporation, or magnetron sputtering in glancing angle deposition (GLAD) geometry can be used to fabricate fancy porous microstructured thin films. Several reviews have been written on this topic focusing either on the physics of the deposition process [1,2] or the optical performance [3, 4] and other potential applications of the deposited porous materials [5,6].

One of the most interesting effects of GLAD is the capability to grow strongly birefringent or dichroic coatings because of the possibility to control the anisotropic microstructure of the deposited materials. Thus porous columnar thin films (CTF) or more sophisticated sculptured thin films (STF) can be manufactured to work as retarders [7], mirrors showing circular Bragg phenomenon [8,9], omnidirectional reflection mirrors [10], or tunable circular polarizers [11]. However, a commonly claimed drawback for the implementation of nanostructured GLAD thin films as reliable optical elements is precisely their high porosity and their associated optical instability due to ambient water vapor adsorption and condensation in the pores.

The motivation of this work is to convert this weakness in a strength for the development of label free vapor and liquid sensing devices based on a tunable fluidic actuated optics. Vapor or fluid sensors based on porous thin films have been proposed in the literature [12,13,14]. More specifically, fluid sensors have been proposed previously by Lakhtakia et al. [15], high speed optical humidity sensors have been developed by Liu et al. [16] and several other authors have applied optically complex GLAD structures for the monitoring of liquids or vapors using different methods of interrogation [6]. In previous works we have also shown that 1D-photonic crystals and Bragg Microcavities (BM) formed by the successive stacking of porous TiO_2 and SiO_2 CTFs deposited by electron beam evaporation in a GLAD geometry change their optical behavior when

they are infiltrated with liquids [17,18,19]. This response was dependent on the refractive index of the infiltrated liquid and we proposed using this effect for liquid monitoring [18]. An outstanding possibility by the fabrication of these structures is to make them either optically active or inactive with respect to the polarization of light [19], a feature that has not been used previously in a systematic way for liquid or vapor detection. Thus, in the present work we provide a deeper insight into the birefringence behavior of some porous sculptured BM prepared by GLAD and discuss how to benefit from the ability of tuning their optical anisotropy to develop robust, cheap and reliable optofluidic transducers that, incorporated into microfluidic chips, serve to monitor vapors and liquid solutions.

2 Fabrication of birefringent thin film optical elements with open porosity

In general, glancing angle deposition of a vapor flux at low enough process pressures give rise to porous thin film growth with open porosity and anisotropic microstructure. If the mobility of the deposited moieties of material is weak, open regions are formed by the shadowing of the initial nucleation centers to the arriving flux of material. In the incidence plane (formed by the flux direction and normal to the sample surface) the competition between this shadowing mechanism and adatom mobility leads to the growth of tilted nanocolumns. On the other hand, in the direction perpendicular to the incidence plane, there is no shadowing and a homogeneous supply of vapor takes place. Thus, the columns fan out laterally due to the lack of shadowing perpendicular to the deposition plane inducing an enhanced connectivity of the deposited material in this direction. This anisotropic column aggregation is known as bundling. This phenomenon was thoroughly discussed

in ref.[1]. Figure 1a (plane of incidence) and 1b (front view) shows a scheme of the deposition process and an ideal scheme of the developed thin film microstructure.

If no movement is applied to the substrate during the GLAD of a thin film (as it is assumed in the description below), tilted columnar growth takes place. In general, this tilted columnar growth is considered a disadvantage for the development of optically active elements that are going to operate at normal incidence of the light. This is due to the fact that standard isolated nanocolumn arrays present limited in-plane birefringence Δn, defined this as the difference in effective refractive index for light incidence normal to the surface for polarizations either parallel n_p or perpendicular n_s (bundling direction) to the plane of incidence (p and s directions in Figure 1b, respectively).

In a 3D coordinate system (Figure 1a, $n_s = n_3$ and $n_p = 1/\mathrm{sqrt}(\sin^2\psi/n_1^2+\cos^2\psi/n_2^2)$ where ψ is the column tilt angle, and n_1, n_2 and n_3 the principal refractive indices of the film (n_1 along the column direction, n_2 in the direction perpendicular to the column direction in the plane of incidence and n_3 in the direction perpendicular to the deposition plane, see figure 1). Taking into account depolarization factors within an effective medium approximation it is expected that $n_1 < n_3 < n_2$. This situation can be modified varying the standard GLAD protocol. Thus, for example, the so-called serial bideposition [20], the use of substrates with a patterned surface or the use of increased

process pressures may alter the lateral interconnection of material and therefore, the columnar growth to enhance in-plane birefringence.

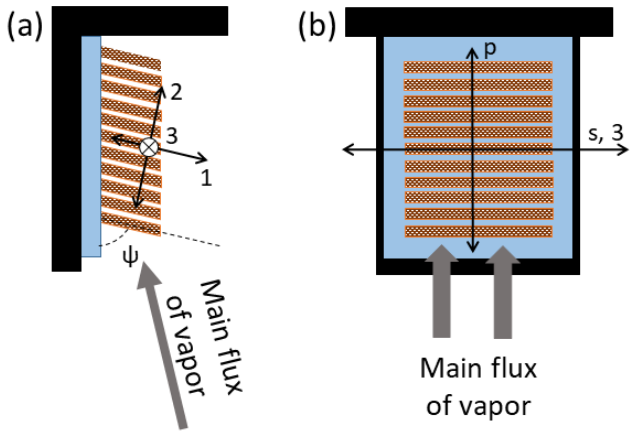

Fig 1. Scheme of GLAD deposition process used in this work and developed thin film microstructure. (a) Plane of incidence and tilted thin film columnar growth (main optical axis of CTF are included). (b) Lateral columnar association in the direction s perpendicular to the plane of incidence.

3 Sensing with birefringent porous BM optical elements

Although individual single material GLAD thin film architectures can be used to fabricate vapor or liquid sensing elements, we will show that the traditional optical multilayer design combined with CTF porous materials of different refractive index can be effectively used to develop optical devices with enhanced sensitivity and robustness. In particular, BMs are especially suited for the development of sensing elements. A BM consists of two Bragg mirrors separated by a central layer (cavity) whose thickness and refractive index is chosen to open a narrow transmission peak (defect peak) at the reflection band of the Bragg mirrors.

In this paper we report on sculptured porous BMs fabricated by the successive stacking of SiO_2 and TiO_2 CTF prepared by GLAD electron beam evaporation of SiO_2 or TiO pellets, respectively. The zenithal angle of evaporation was 70º. The Bragg reflectors consists of seven stacked CTFs

of SiO_2 and TiO_2 (individual thicknesses of ~80 nm) sandwiching the thicker (~180 nm) SiO_2 CTF cavity as indicated by the figure 2a. The thickness of the individual layers was controlled by a calibrated quartz microbalance. Azimuthally turning the substrate by 180º for each deposited layer rendered a zig-zag columnar microstructure and a homogeneous thickness over relatively large areas. The base pressure of the deposition equipment was $1.0x10^{-6}$ mbar and the process pressure during film growth was $2x10^{-4}$ mbar by intake of a O_2 leak to the chamber to warrant that the samples grow transparent (i.e., fully oxidized). The crucible-sample distance was about 50 cm, the deposition rate about 6 nm per minute, and the sample temperature during growth about 100ºC.

The resulting zig-zag microstructure is clearly devised in the micrograph of Figure 2a-left corresponding to a FIB-SEM cross section taken normal to the surface along the p direction (i.e., perpendicular to the bundling direction, see inset). Meanwhile, the FIB-SEM taken along the s direction (Figure 2a-right) shows that the nanocolumns are laterally associated (note the higher connectivity of the deposited material in this direction with respect to that in Figure 2a-right) and that this association covers the whole multilayer structure, i.e., it passes from one layer to the next even if the deposited materials are different. We have named this lateral association of nanocolumns comprising the whole thickness of the BM and affecting different material layers as fence-bundling [19].

Figure 2b shows the transmittance at normal incidence of polarized light through the sculptured zig-zag BM. Note that the transmitted defect peak (in this case at 590-620 nm) varies its position and intensity depending on the orientation of the light polarization vector with respect to the optical axes of the sample. Thus, if the polarization of the light is aligned to the p axis of the sample, the transmitted peak is shifted by 23 nm to lower wavelength than for the alignment along the s axis.

For intermediate orientations, a double peak is transmitted, confirming the birefringent behavior of the BM. Note that this birefringence has structural origin.

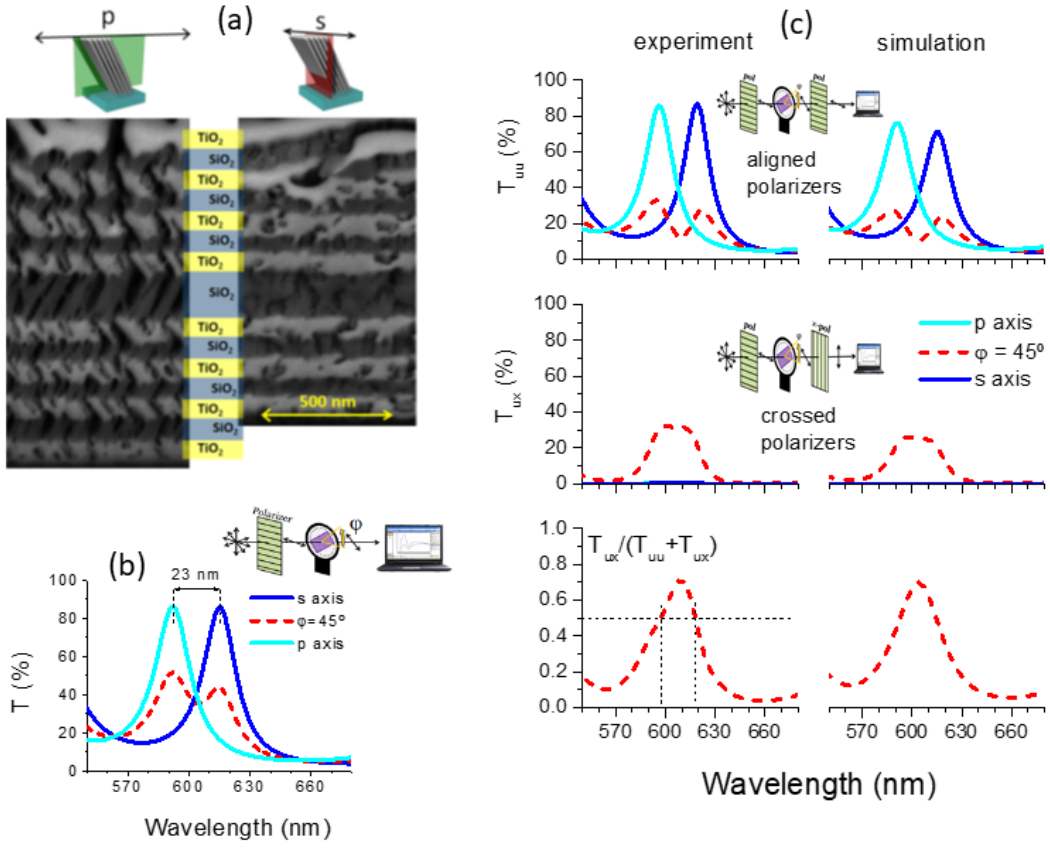

Fig 2. a) Cross section FIB-SEM micrographs (left p-axis, right s-axis) of the sculptured BM. b) Experimental transmittance T of polarized light at normal incidence of the BM around its defect peak c) Experimental measurements (left) and simulations (right) of transmittance after aligned T_{uu} (top) or crossed T_{ux} (middle) polarizers of the BM for incident light normal to the surface and polarization parallel to s, p or φ=45º azimuthal sample orientations. The corresponding intensity ratios between these signals are also shown (bottom).

To quantify the optical response of the BM we have developed an optical model to simulate the optical behaviour of this porous sculptured BM. For simplicity, we took each layer within the BM as a porous uniaxial birefringent media. A good consistency with experimental transmittance

measurements was achieved considering a multilayer optical model with in-plane birefringence of $\Delta n=0.150$ for the TiO_2 layers and 0.043 for the SiO_2 layers of the BM. Note that these values are about the same than those reported for the same materials deposited as single layer in a serial bideposition process [20]. The consistency of the optical model is demonstrated by the equivalence of the experimental and simulated transmitted spectra reported in Figure 2c. In this experiment, normal incident polarized light impinges onto the sculptured BM and the transmitted light is analyzed with a second polarizer aligned either parallel (T_{uu}) or perpendicular (T_{ux}) to the polarization vector of the incident light for three azimuthal sample orientations: parallel to s, p or 45º off these main axes (i.e., azimuthal angle $\varphi = 45º$, see inset).

The spectra reported in this figure can be interpreted in the following terms. For aligned polarizers and azimuthal sample orientation $\varphi=45º$, two resonant peaks are generated (red dashed curves in the top panel of Figure 2c) and their separation can be taken as a measure of the optical activity of the system. By contrast, for the polarization vector of the incident light aligned parallel to the s or p azimuthal sample axis, a single defect peak located at different wavelengths was found. One of these peaks appears when the polarization vector of the impinging light aligns with the s sample direction and light travels through the slow optical axis (i.e., parallel to the bundling and presenting a higher refractive index), while the second occurs when the light travels through the fast optical axis with the polarization aligning the p direction (i.e., perpendicular to the bundling). The separation between these two single peaks is 23 nm, a displacement stemming from the combined effect of the optical transmittance of the sculptured BM and the different polarizability of the individual layers for the two optical axis. In particular, we link the observed higher polarizability in the single layers (and therefore a refractive index larger than in the orthogonal direction) to the enhanced connectivity of the material in this direction as observed in the FIB-SEM micrographs

of Figure 2. Other consequences of the birefringence of the BMs reported in Figure 2c refers to the results gathered in the middle and bottom panels. In concrete, when using crossed polarizers (i.e., T_{ux}), transmitted intensity was only observed when the optical axes of the sample are misaligned with respect the polarization of the incident light, reaching a maximum value for an orientation of the sample optical axis of 45º off the polarization of the incident light beam. It is noteworthy that the sculptured BM optically characterized in figure 2 acts as a quarter waveplate (i.e., when $T_{uu} = T_{ux}$) at $\varphi = 45º$ and wavelengths of 595 and 620 nm.

a) Vapor sensing

The previous analysis was performed with "as prepared" sculptured BMs, i.e., with their pores filled with air. According to effective medium theories, it is a reasonable assumption that the difference in polarizability between the s and p sample axis vary, as the open sample pores are partially or completely filled with condensed vapors or liquids. In the following, we describe how we can take advantage of this phenomenon for the development of effective vapor and liquid sensors based on the optically active sculptured BM herewith discussed. It will be also shown that optical interrogation can be done by either transmission or reflection geometries, this latter opening the way for the use of these BMs as optofluidic transducers at the tip of optical fibers.

Acetone vapor sensing experiments with the BM transducer were carried out in reflection mode. The geometry of the experimental set-up is outlined in the scheme of Figure 3a and a picture of the actual device is shown in Figure 3b. Polarized light is sent to the back side of the substrate with an angle of incidence of 75º. The porous sculptured BM transducer is placed facing the vapor source. The specular reflected light is analyzed with a second polarizer aligned parallel or crossed with respect to the polarization of the incident light. The sample optical axes are aligned 45º off

the orientation of the polarizers. Using these working conditions, the BM was exposed to various partial pressures of acetone vapors by regulating its distance to the liquid level of a Beaker glass containing 50 cc of acetone. Reflected spectra were acquired at several distances between the acetone level and the BM with the orientation of the polarizers either aligned or crossed. Figures 3c and 3d show the reflectance spectra of the resonant peak recorded, respectively, with aligned R_{uu} or crossed R_{ux} polarizers as the transducer approaches the acetone level. Short acquisition times (few minutes) for the full series of advancing or receding spectra were used to minimize the eventual change of liquid height in the glass due to evaporation. Figures 3e and 3f show the quantification (peak position, width, and intensity) when the BM transducer approaches or recedes the acetone level.

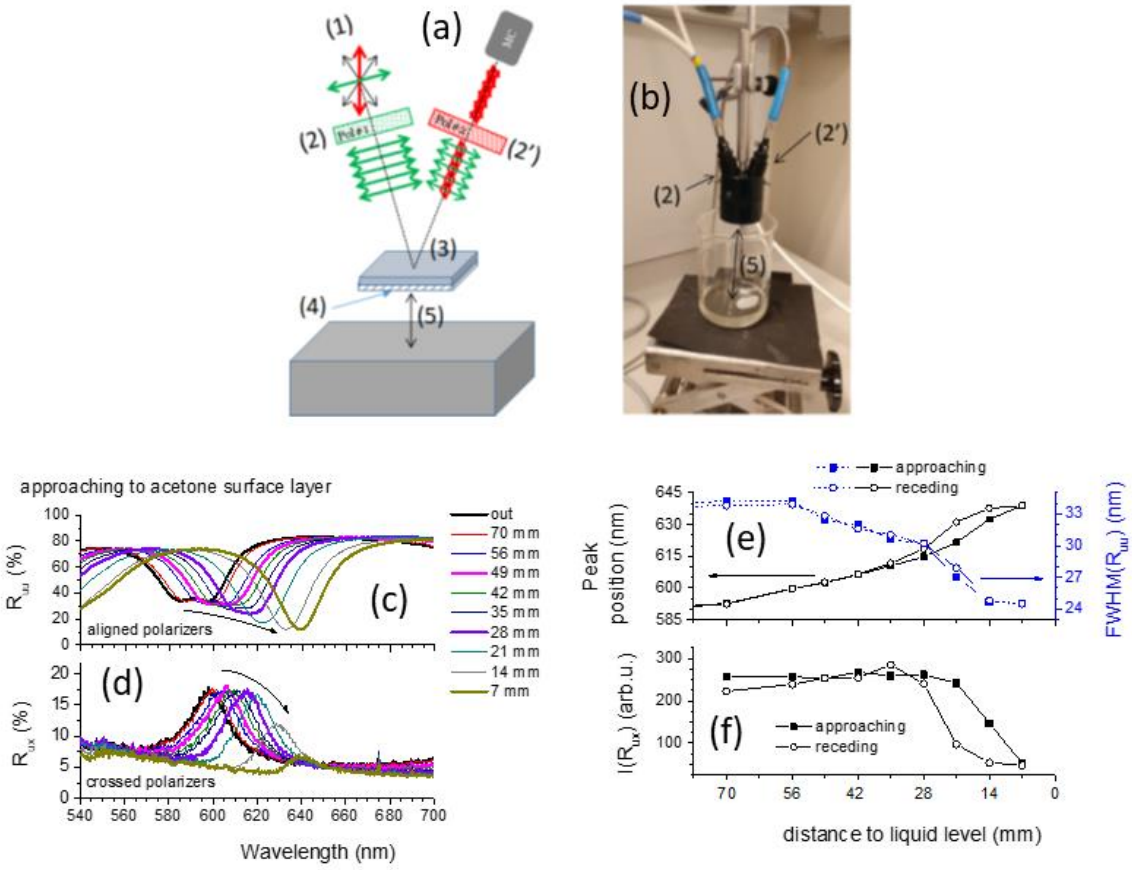

Fig 3. Scheme of the set-up used for vapor sensing in reflection mode (a) and picture of the experimental arrangement (b): (1) light source, (2) (2') polarizers, (3) substrate, (4) BM transducer, (5) transducer liquid level distance. Reflectance measurements through aligned R_{uu} (c) or crossed R_{ux} (d) polarizers at several distances between the sculptured BM and the acetone level, as it approaches to the liquid level. (e) peak position (left axis), full width at half maximum (right axis) of the resonant peak and (f) intensity of the defect peak after crossed polarizers $I(R_{ux})$ at several distances BM-acetone level, for the BM approaching (full symbols) or receding (hollow symbols) from the liquid level.

The reported spectra show the expected resonant peak shift resulting from the progressive filling of the BM pores with condensed acetone vapor as its partial pressure increases towards the liquid surface [21]. In addition, changes in shape and intensity, resulting from the tuning of the

birefringence of the sculptured BM transducer, take place. Since these latter effects are the main novelty of the proposed analysis, we will further discussed the involved phenomenology. Figure 3c reveals a progressive redshift in the position of the double R_{uu} resonant deep and a merging of the two components into one, particularly for distances liquid-transducer smaller than 35 mm. Correlated with this peak merging, Figure 3d shows an identical progressive redshift of the resonant peak after cross polarizers R_{ux} and a decrease of intensity of the reflected resonant peak for the shortest acetone-transducer distances. The process was reversible, though presenting some hysteresis, and the spectrum progressively recovered the initial shape and position when withdrawing the BM from the acetone. Figure 3e presents the position and the full width at half maximum (FWHM) of the resonant peak in Figure 3c, and Figure 3f the intensity of the resonant peak after cross polarizers $I(R_{ux})$, as the transducer approaches (full symbols) or recedes (hollow symbols) from the liquid level. According to our assumption of a progressive filling of the BM pores with condensed vapor of acetone, the initial red shift of the resonant peak taking place without a significant variation of the width and intensity of the resonant peak is consistent with the filling of micropores existing inside the nanocolumns [17], while the mesopores between the bundling arrangement of the nanocolumns remain still empty. As the acetone vapor pressure increases by approaching the BM to the surface level, the two resonant peak components start to merge into a single component, a sign of the progressive loss of the birefringence of the system. We assume that under these conditions acetone is condensing in the mesopores and complete their filling for a separation between the transductor and the acetone level of 7 mm or less. Beyond this point, no further redshift or peak shrinking was detected, suggesting that the open pores of the BM have been completely filled with condensed acetone. It is also noteworthy that the receding curve shows a certain hysteresis that reminds the typical shape of adsorption isotherms of mesoporous

materials [22] and that indicate a certain restriction for the ease of the vapors condensed in the pores.

A first consequence of this experiment is that the sculptured BM can be used as vapor sensors by following the changes in resonant peak upon condensation into the pores. Similar analyses have previously been done by other authors following the shift of transmission or reflection peaks or bands [15, 21], but not changes in the shape and intensity of the resonant peak of a porous BM as proposed here by monitoring the optical changes with linearly polarized light.

The obtained results support the existence of two types of pore sites within the BM. Micropores located within the nanocolumns whose filling does not affect significantly the in-plane birefringence of the system and mesopores between the columnar bundling arrangement whose filling decreases the optical activity of the system. In this regard, the series of spectra in Figure 3d taken with crossed polarizers provide additional information about the outlined progressive loss of optical activity when the larger pores of the system become filled with condensed vapors. Besides the expected redshift, the spectra taken at the shortest distances from the liquid surface reveals a drastic decrease in $I(R_{ux})$ intensity, which clearly confirm the loss of birefringence. From a practical point of view, the high sensitivity for detecting retardance changes following the variations in $I(R_{ux})$ (there is a factor 5 difference between the BM empty and fully filled of condensed acetone) supports the possibility of directly detecting vapor pressure changes with the sculptured BM transducer and a simple photodiode to measure light intensity. Note that this monitoring approach is quite straightforward because it is simpler and more robust than following a peak position. We will come back to this point in the next section where we discuss the use of the optically active sculptured BM for liquid sensing applications.

b) Microfluidic liquid sensing

The optically active BM hitherto described can also be used for microfluidic label free liquid sensing. In fact, the open porosity of these optical elements offers the possibility to develop robust sensing devices by flowing liquids through its structure. In particular, a possibility that we have explored is the incorporation of the BM into microfluidic chips to determine changes in refractive index of liquids in a continuous way. The experimental set-up is similar to that shown in Figure 3a and b regarding the detection system, but in this case the sculptured BM transducer was encapsulated within a microfluidic chip (c.f. ref.[18]) to allow easy liquid circulation within its porous structure. This feature would be quite useful to monitor the evolution of liquid characteristics in fermentation processes, salinity variations or hydrocarbon mixtures and other similar applications. To explore the liquid sensing capacity of the optically active BMs, we have analyzed the spectral evolution when this structure was immersed in glucose aqueous solutions of different concentrations. For this aim several distilled water glucose (purity >99.5% Sigma-Aldrich) solutions were prepared. The transducer was initially cleaned by flowing distilled water through their porosity. No further cleaning was made for the series of characterization made for the series of solutions with different amount of glucose. Figure 4a shows a series of reflectance after crossed polarizers R_{ux} measurements and Figure 4b shows the variation of intensity ratio $I(R_{ux})/I(R_{uu})$ for several aqueous glucose solutions infiltrated within the pores of the BM. Regarding the sensitivity of the measurement system, it is noteworthy in this plot that a variation of 0.06 refractive index units (RIU) in the aqueous glucose solution (as it is the case between solutions of 0.0% and 36% brix; 1% brix = 1 gr sugar / 100 gr solution) corresponds to about a factor two of the $I(R_{ux})/I(R_{uu})$ ratio. Moreover, under the conservative assumption that differences in intensity ratio $I(R_{ux})/I(R_{uu})$ of 0.5% can be followed in this experiment, the system would be able to discern changes in 0.2% brix or 0.0003 RIU, similar to the sensitivity of any standard

refractometer. This corresponds to a sensitivity defined as intensity modification per refractive index unit of ~1660/RIU. The absence of any hysteresis as in the case of vapor sensing described above, further support the reliability of the liquid sensing process based on the optically active BM.

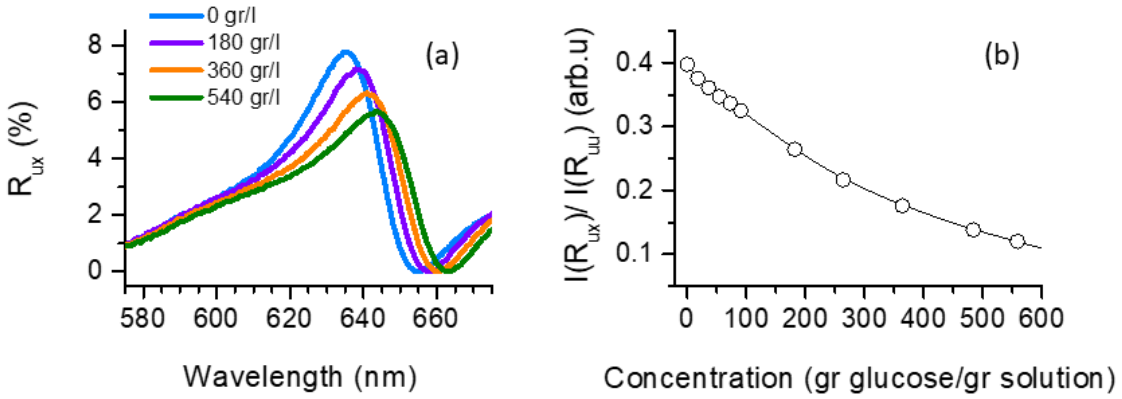

Fig 4. a) Experimental measurement of the reflectance after cross polarizers R_{ux} and (b) intensity ratio of the reflected defect peaks $I(R_{ux})/I(R_{uu})$ in the porous BM transducer as the concentration of glucose in the solution increases

To probe the capability of the previous measurement procedure for real microfluidic applications we have developed an integrated microfluidic system. The scheme of the optical part of the apparatus is drawn in figure 5a and a picture of the actual prototype is presented in figure 5b (a patent claim protects this device and measurement system [23]. It is based on the evaluation of the change of the optical activity of the resonant peak of a porous sculptured BM when the liquid solution circulates through the sample pores. The optical part of the system, schematically presented in Figure 5a, consists of a beam of polarized light that impinges normal to the surface of a fluidic device that contains the BM. The light is supplied by a LED with a wavelength selected

to match the resonant peak of the optically active BM. In the scheme of the figure, the system works in transmission, and the polarization state of the transmitted light is analyzed with a polarizing beamsplitter cube that separates polarized light in their two components. An alternative design also exists for a reflection geometry. A virtue of this optical arrangement is to minimize/avoid the use of complex and expensive optical elements (light sources, wavelength analyzing tools, monocromators, or ellipsometers). The simple device is capable of following the evolution of the fermentation process without directly measuring the refractive index of the solution and without requiring an accurate description of the optical parameters of the BM. The measurement relies on determining the variation of the intensity ratio of the BM resonant peak I_{ux}/I_{uu} asa function of the characteristics of the liquid. This allows an easy implementation together with common electronic appliances.

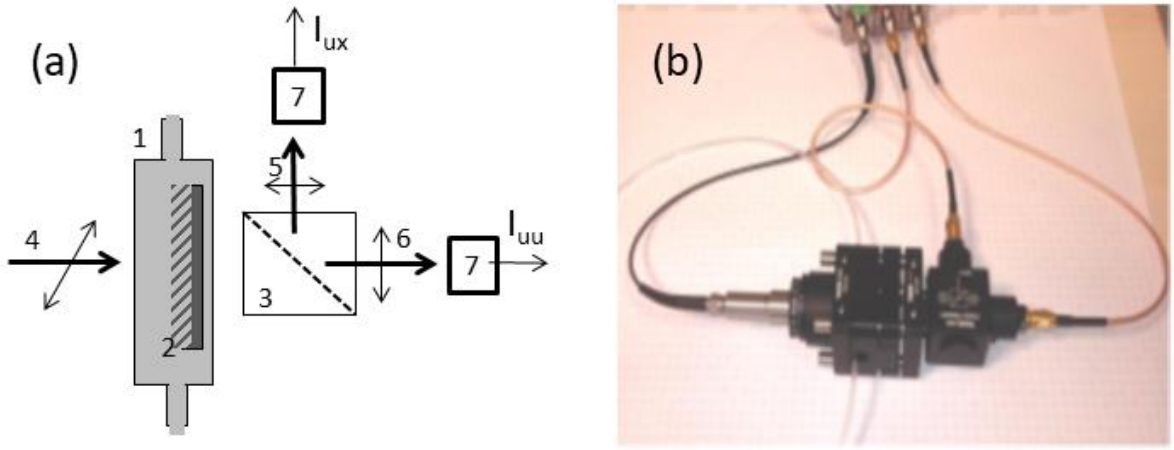

Fig 5. a) Scheme of optical design of microfluidic system for label free liquid sensing: 1 microfluidic chip, 2 porous sculptured BM transductor, 3 polarizing beamsplitter cube, 4 polarized light, 5 and 6 the two components of the polarized light after interaction with the transductor, 7 photodiodes. b) Manufactured prototype

4 Summary

Porous sculptured Bragg microcavities prepared by e-beam evaporation GLAD by the stacking of successive layers of SiO_2 and TiO_2 with a zig-zag structural configuration present tunable birefringence (and therefore optical activity) when infiltrated with condensed vapors or liquids so they can be used as transducers for label free vapor and liquid sensing. The outstanding microstructural characteristics of their individual layers, their porosity and the lateral aggregation of their nanocolumns (defined as fence-bundling) confers them a tunable optical activity and the capacity to act as transducers for label free vapor and liquid sensing. We show that the change in birefringence upon condensed vapor infiltration can be used to follow hysteresis loops usually observed in adsorption isotherms, or to monitor the evolution of solutions of varying refractive indices.

Acknowledgments

We thank Spanish Ministry of Economy, Industry and Competitiveness (AEI-FEDER project MAT2016-79866-R, CSIC 201560E055) for financial support.

References

1. H. van Kranenburg, C. Lodder "Tailoring growth and local composition by oblique-incidence deposition: a review and new experimental data" *Materials Science and Engineering Rll* 295-354 (1994) [doi:10.1016/0927-796X(94)90021-3]
2. A. Lakhtakia, R. Messier, *Sculptured thin films, nanoengineering morphology and optics*, SPIE Press (2005)

3. M.M. Hawkeye, M.T. Taschuk, M.J. Brett, Introduction: Glancing Angle Deposition Technology, in Glancing Angle Deposition of Thin Films: Engineering the Nanoscale, John Wiley & Sons, Ltd, Chichester, UK. (2014) [DOI: 10.1002/9781118847510.ch1]
4. M.W. McCall, I.J. Hodgkinson, Q. Wu, *Birefringent thin films and polarizing elements*, Imperial College Press 82015)
5. M. Suzuki, "Practical applications of thin films nanostructured by shadowing growth" *J. of Nanophotonics* 073598 (2013) [doi:10.1117/1.JNP.7.073598]
6. A.R. González-Elipe, A. Barranco, A. Borras, A. Palmero, "Perspectives on oblique angle deposition of thin films: From fundamentals to devices" *Progress in Materials Science* 76, 59-153 (2016) [doi: 10.1016/j.pmatsci.2015.06.003]
7. R.J. Martin-Palma, f. Zhang, A. Lakhtakia, A. Cheng, J. Xu, C.G. Pantano, "Retardance of chalcogenide thin films grown by the oblique-angle-deposition technique", *Thin Solid Films* 517, 5553 (2009) [doi:10.1016/j.tsf.2009.03.200]
8. P.D. McAtee, A. Lakhtakia, "Reflection and transmission of obliquely incident light by chiral sculptured thin films fabricated using asymmetric serial-bideposition technique". *J. Nanophotonics* 11, 043502 (2017) [doi:10.1117/1.JNP.11.043502]
9. I Hodgkinson, Q. H. Wu, B. Knight, A. Lakhtakia, K. Robbie, Vacuum deposition of chiral sculptured thin films with high optical activity, *Appl. Optics* 39, 642 (2000) [doi: 10.1364/AO.39.000642]
10. V. Leontyev, M. Hawkeye, A. Kovalenko, M.J. Brett, "Omnidirectional reflection from nanocolumnar TiO2 films", *J. Appl. Phys*. 112, 084317 (2012) [doi:10.1063/1.4759138]
11. K.M. Krause, M.J. Brett, Spatially graded nanostructured chiral films as tunable circular polarizers. *Adv. Func. Mat.* 18 , 3111 (2008) [doi:10.1002/adfm.200800685].

12. M.E. Calvo, S. Colodrero, N. Hidalgo, G. Lozano, C. Lopez-Lopez, O. Sanchez-Sobrado, H. Mıguez, "Porous one dimensional photonic crystals: novel multifunctional materials for environmental and energy applications", *Energy Environ. Sci.* 4, 4800 (2011) [doi:10.1039/C1EE02081A]
13. K. Szendrei , P. Ganter , O. Sànchez-Sobrado , R. Eger , A. Kuhn , B.V. Lotsch , "Touchless Optical Finger Motion Tracking Based on 2D Nanosheets with Giant Moisture Responsiveness", *Adv. Mater.* 27, 6341–6348 (2015) [doi:10.1002/adma.201503463]
14. P. Ganter, K. Szendrei, B.V. Lotsch, "Towards the Nanosheet-Based Photonic Nose: Vapor Recognition and Trace Water Sensing with Antimony Phosphate Thin Film Devices" *Adv. Mater.* 28, 7436–7442 (2016) [doi:10.1002/adma.201601992]
15. A. Lakhtakia, M.W. McCall, J.A. Sherwin, Q.H. Wu, I.J. Hodgkinson, Sculptured thin film spectral holes for optical sensing of fluids, Optics Comm. 194 (2001) 33 [doi: 10.1016/S0030-4018(01)01225-1]
16. Y.J. Liu, J.Shi, F. Zhang, H. Liang, J. Xu, A. Lakhtakia, "High-speed optical humidity sensors based on chiral sculptured thin films". *Sensors and Actuators B* 156, 593 (2011) [doi:10.1016/j.snb.2011.02.003].
17. L. Gonzalez-Garcia, G. Lozano, A. Barranco, H. Mıguez, A.R. Gonzalez-Elipe TiO2–SiO2 "One-dimensional photonic crystals of controlled porosity by glancing angle physical vapour deposition" *J. Mater. Chem.* 20, 6408–6412 (2010) [doi:10.1039/c0jm00680g]
18. M. Oliva-Ramirez, L. González-García, J. Parra-Barranco, F. Yubero, A. Barranco, A.R. González-Elipe, "Liquids Analysis with Optofluidic Bragg Microcavities" *ACS Applied Materials and interfaces* 5, 6743 (2013) [doi: 10.1021/am401685r]
19. M. Oliva-Ramirez, A. Barranco, M. Loffler, F. Yubero, A.R. González-Elipe, Optofluidic Modulation of Self-associated nanostructural units forming planar Bragg microcavities *ACS Nano* 10, 1256 (2016) [doi:10.1021/acsnano.5b06625]

20. I. Hodgkinson, Q.H. Wu Serial bideposition of anisotropic thin films with enhanced linear birefringence Appl. Opt. 38, 3621 (1999) [doi: 10.1364/AO.38.003621]
21. M.M. Hawkeye, M.J. Brett, Optimized Colorimetric Photonic-Crystal Humidity Sensor Fabricated Using Glancing Angle Deposition, Adv. Funct. Mater. 21, 3652 (2011) [doi: 10.1002/adfm.201100893]
22. S.J. Gregg, K.S.W. Sing, "Adsorption, Surface Area and Porosity"; Harcourt Brace and Co.: Orlando, FL, (1997).
23. M. Oliva-Ramírez et al. "Sensor, apparatus, and method for determining a concentration of solute in a solution". Patent application number PCT/ES2016/070764; publication number: WO2017072388 A1 .

Manuel Oliva-Ramirez received his Ph.D. degree in Material Science from the University of Seville in 2016. His research was related to the design and fabrication of nanostructured porous thin films of different oxides for their implementation in optofluidic and photovoltaic devices. He is currently a postdoctoral researcher at the Leibniz-Institute for New Materials in Saarbruecken working on the development of conductive composites.

Jorge Gil-Rostra received his degree in Chemistry from de University of Burgos in 1998 and his Ph. D. degree in Materials Science from the University of Seville in 2013. From 1998 to 2007 he has worked as responsible of Surface Treatments and Quality Manager at several Spanish companies. Since 2007 he works as a researcher at the Institute of Materials Science of Seville. His main research interest focus on magnetron sputtering deposition methods, mixed oxides thin films, luminescent materials, and optofluidic devices.

Agustin R. González-Elipe is Research Professor of CSIC at the Institute of Materials Science of Seville. He is expert in thin film technology and plasma and vacuum deposition methods that, among other applications, he has used for the fabrication of photonic sensor films and optofluidic detection systems. He is author or co-author of more than 400 publications and author and editor of several books and reviews on thin film growth and applications.

Carmen López-Santos is a postdoctoral researcher at the Institute of Materials Science of Seville (Spain). She received her BS degree in physics and her PhD degree from the University of Seville in 2004 and 2009, respectively. Her current research interests include surface modification by plasma and vacuum technologies for multifunctional applications of photoactive oxides, anisotropic nanostructures, biomaterials and protective coatings with antifreezing properties.

Francisco Yubero received his Ph.D. degree in physics at the Universidad Autónoma de Madrid in 1993. Since 1996, he is a Research Scientist from CSIC at the Instituto de Ciencia de Materiales

de Sevilla. His research focuses on theoretical aspects related to surface electron spectroscopies and the practical implementation of functional thin films into technological devices.

Caption List

Fig 1. Scheme of GLAD deposition process used in this work and developed thin film microstructure. (a) Plane of incidence and tilted thin film columnar growth (main optical axis of CTF are included). (b) Lateral columnar association in the direction s perpendicular to the plane of incidence.

Fig 2. a) Cross section FIB-SEM micrographs (left p-axis, right s-axis) of the sculptured BM. b) Experimental transmittance T of polarized light at normal incidence of the BM around its defect peak c) Experimental measurements (left) and simulations (right) of transmittance after aligned T_{uu} (top) or crossed T_{ux} (middle) polarizers of the BM for incident light normal to the surface and polarization parallel to s, p or φ=45º azimuthal sample orientations. The corresponding intensity ratios between these signals are also shown (bottom).

Fig 3. Scheme of the set-up used for vapor sensing in reflection mode (a) and picture of the experimental arrangement (b): (1) light source, (2) (2') polarizers, (3) substrate, (4) BM transducer, (5) transducer liquid level distance. Reflectance measurements through aligned R_{uu} (c) or crossed R_{ux} (d) polarizers at several distances between the sculptured BM and the acetone level, as it approaches to the liquid level. (e) peak position (left axis), full width at half maximum (right axis) of the resonant peak and (f) intensity of the defect peak after crossed polarizers I(R_{ux}) at several distances BM-acetone level, for the BM approaching (full symbols) or receding (hollow symbols) from the liquid level.

Fig 4. a) Experimental measurement of the reflectance after cross polarizers R_{ux} and (b) intensity ratio of the reflected defect peaks $I(R_{ux})/I(R_{uu})$ in the porous BM transductor as the concentration of glucose in the solution is increases

Fig 5. a) Scheme of optical design of microfluidic system for label free liquid sensing: 1 microfluidic chip, 2 porous sculptured BM transductor, 3 polarizing beamsplitter cube, 4 polarized light, 5 and 6 the two components of the polarized light after interaction with the transductor, 7 photodiodes. b) Manufactured prototype